Magazine of Concrete Research, 2010, **62**, No. 8, August, 557–567
doi: 10.1680/macr.2010.62.8.557

A generalisation of the Hillerborg's model for the analytical evaluation of ductility of RC beams in bending

E. Cadamuro, A. Carpinteri and M. Paggi

Politecnico di Torino

In this study, a generalised analytical model for the evaluation of the plastic rotations of reinforced concrete beams in bending is proposed. To this aim, the pioneering Hillerborg's model is here extended by taking into account also the contribution of reinforcement in compression. Moreover, a detailed comparison with the experimental results by Bosco and Debernardi on three-point bending reinforced concrete beams by varying the reinforcement percentage and the size-scale of the structural elements is carried out. This permits study of the influence of the parameter β, related to the length of strain localisation of concrete in compression, on the ductility response and how to tune this parameter according to experiments. The proposed generalisation of the Hillerborg model is then suitably applied to over-reinforced concrete beams in bending, where concrete crushing is the prevailing non-linearity; it is shown that the model is able to capture the phenomenon of size-scale effects.

Introduction

Modelling the mechanical behaviour of the constituent materials is of central importance in the analysis of the flexural behaviour of reinforced concrete (RC) beams. The constitutive law of concrete in tension is usually defined according to the cohesive model (Carpinteri, 1984; Hillerborg, 1990) as a pair of constitutive laws: a linear–elastic stress–strain relationship before achieving the material tensile strength and a linear-softening stress–crack opening displacement relationship for the cracked phase. When the ultimate strength is achieved, strain localises and the decreasing stress–strain branch depends on the length of the base of measurement (Carpinteri, 1984, 1989).

On the other hand, with reference to the behaviour of concrete in compression, Hillerborg (1990) first proposed an analytical model based on the phenomenon of strain localisation of the cementitious material in compression. According to this approach, strain localisation takes place when the ultimate compressive strength is achieved and, for a beam with rectangular cross-section, it develops on a characteristic length ℓ which, evaluated along the axis of the beam, is estimated to be nearly proportional to the height of the compressive zone, x, in the cross-section. This assumption was put forward by Hillerborg and is corroborated by comparisons with finite-element analyses and with measured curves in pure compression according to van Mier (1984). This law of proportionality is expressed by a factor which was assumed by Hillerborg to be equal to 0·8, as can be seen in Figure 1.

Following this analytical model, it is possible to define a stress–strain law for concrete in compression

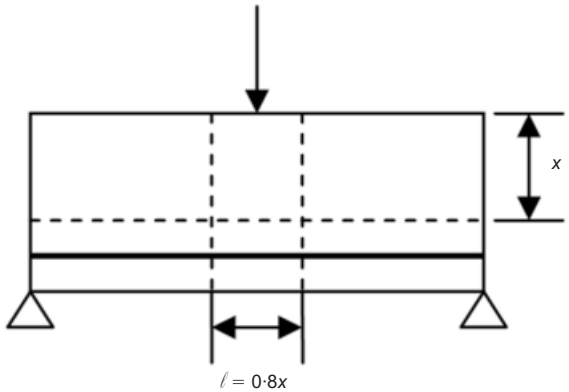

Figure 1. Schematic representation of the beam element

Politecnico di Torino, Department of Structural and Geotechnical Engineering, Corso Duca degli Abruzzi 24, 10129 Torino, Italy

(MACR 900099). Paper received 16 June 2009; accepted 4 December 2009

www.concrete-research.com 1751-763X (Online) 0024-9831 (Print)

before the achievement of the ultimate compressive strength and a stress–displacement law after this peak. Actually, these two laws can be unified in a complete bilinear stress–strain law, where the strain is given by the addition of a contribution relative to the undamaged phase and another relative to the damaged phase. The latter is given by the ratio between the displacement and the characteristic length where strain localises. With reference to the Hillerborg's model, the last point of the complete linear stress–strain curve for concrete in compression is inversely proportional to the length of strain localisation zone; that is to the height of the compressive zone, by the coefficient of proportionality which is assumed to be equal to 0·8. This means that the softening post-peak branch and, consequently, the whole constitutive law, varies during the loading process, as it is no longer an intrinsic property of the material. Hillerborg proposed this model for the analysis of size-scale effects on the flexural behaviour of RC beams, although the definition of the value of the characteristic length did not receive an adequate experimental confirmation.

As regards the behaviour of concrete in tension, on the basis of the well-known cohesive crack model (Carpinteri, 1984), when the ultimate tensile strength is achieved, strain concentrates in a localised band which will then develop into a crack, characterised by a stress distribution according to the cohesive law. Since concrete is a quasi-brittle material in tension with an elastic-softening behaviour, the energy dissipation takes place exclusively on the cracked surface. This is rigorously valid only in the absence of volumetric hardening. In fact, in the more general case of elastic, hardening and softening material, the energy is dissipated both in the volume of the undamaged material and on the cracked surface. Whereas the cohesive crack model considers a strain localisation in tension, an analogous behaviour can be observed in compression, as van Mier (1984) found experimentally. On the basis of this observation, Hillerborg (1990) first introduced an analytical model capable of capturing the experimental behaviour.

More recently, a new model has been proposed, the so-called overlapping crack model (Carpinteri *et al.*, 2007), that considers, in analogy with the cohesive model in tension, a pair of constitutive laws for concrete in compression: a linear-elastic stress–strain relationship for the undamaged material, and a softening stress-overlapping displacement relationship for the damaged material. This modelling means that strain localisation of concrete occurs also in compression, that energy dissipates exclusively on the damaged surface and that an interpenetration of the material takes place simulating concrete crushing. Therefore, crushing energy is again an intrinsic property of the material in compression, as is the fracture energy for its tensile counterpart.

Ductility plays a leading role in the flexural design of RC beams and the concept of plastic rotation of a cross-section is used as a driving criterion for quantifying the structural ductility. With reference to a moment–rotation diagram, plastic rotation is given as the difference between final rotation and elastic limit rotation. The experimental research by Bosco and Debernardi (1992), carried out at the laboratory of the department of structural engineering of the Politecnico di Torino, clearly highlighted the size-scale effects on rotational capacity of RC beams in bending, that is a decrease in plastic rotation with the increase in the beam depth.

In the present study, the analytical model by Hillerborg is numerically implemented and, by also taking into account the effect of reinforcement in compression, a detailed comparison with the experimental results by Bosco and Debernardi (1992) is carried out. In fact, the original approach by Hillerborg considered only reinforcement in the tensile zone; on the other hand, since the specimens used by Bosco and Debernardi also present reinforcement in the compressive zone, the Hillerborg model has to be generalised for a correct comparison. More importantly, the effect of confinement due to reinforcement in compression increases the ductile behaviour of RC structures and is an important aspect to be considered.

Beginning from a first theoretical–experimental comparison, where the factor of proportionality 0·8 proposed by Hillerborg is retained, it follows that this coefficient has to be suitably changed in order to match the experimental trends. Moreover, the rotation is not evaluated as the product of a curvature and the characteristic length of crushing, as suggested by Hillerborg, but as the product of a curvature and a length of the specimen chosen equal to its depth, in order to reproduce the testing results of Bosco and Debernardi (1992).

The present study is justified by the opportunity of taking advantage of an analytical model with ease of practical use, generalised also to the case of reinforcement in compression, whose input parameters are tuned on the basis of experimental results featuring the issue of size-scale effects. The last stage is made possible by setting on an experimental basis the factor of proportionality related to the definition of the length of strain localisation of concrete in compression.

Original Hillerborg's model

The Hillerborg (1990) model for the assessment of the behaviour of RC beams in bending is based on the assumptions related to the constitutive laws of the materials composing the RC beams and on the main hypothesis of conservation of plane cross-sections.

On the basis of the hypothesis of partialisation of the cross-section, for which the contribution of the cracked concrete in tension is totally neglected as not reactive,

the analytical approach by Hillerborg (1990) considers a constitutive law for concrete in compression and another for steel in tension. The constitutive law of concrete in compression is characterised by a stress–strain diagram (σ–ε') in which $\varepsilon' = \varepsilon + w/l$, where ε refers to the stress–strain diagram (σ–ε), while w refers to the stress–displacement diagram (σ–w). For a rectangular cross-section, the beam length where the phenomenon of crushing spreads, l, is assumed to be proportional to the depth of the compressive zone, $x = \xi\ d$, multiplied by a factor of proportionality β assumed by Hillerborg to be equal to 0·8

$$l = \beta\ \xi\ d \tag{1}$$

In Equation 1, d is the effective depth evaluated on the distance between the beam extrados and the tensile reinforcement level and ξ is a coefficient of proportionality dependent on the load level and on the steel ratios.

Figure 2 shows the stress–strain diagram proposed by Hillerborg (1990), where ε_1 is defined as

$$\varepsilon_1 = \frac{w_c}{\beta\ d} \tag{2}$$

where w_c is the critical displacement for which the stress is zero.

The reinforcement presents an elastic–perfectly plastic constitutive law as shown in Figure 3. The diagrams of strains and stresses on a rectangular cross-section are shown in Figure 4. With reference to such diagrams, it is possible to write the following equations obtained from similitude of triangles

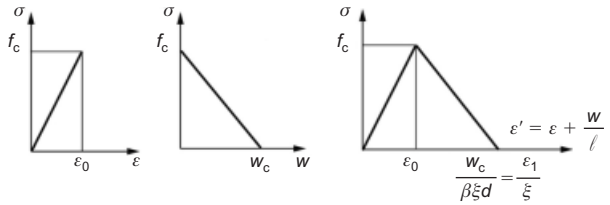

Figure 2. Stress–strain diagram for concrete in compression

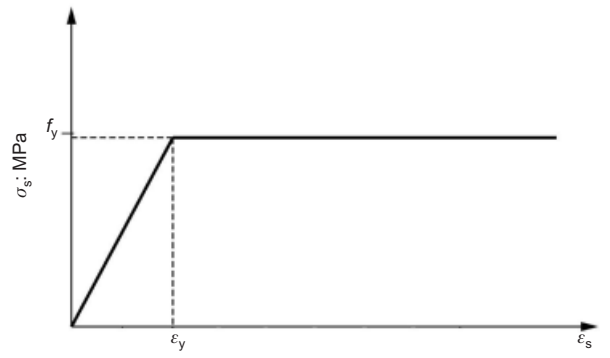

Figure 3. Stress–strain diagram for reinforcement

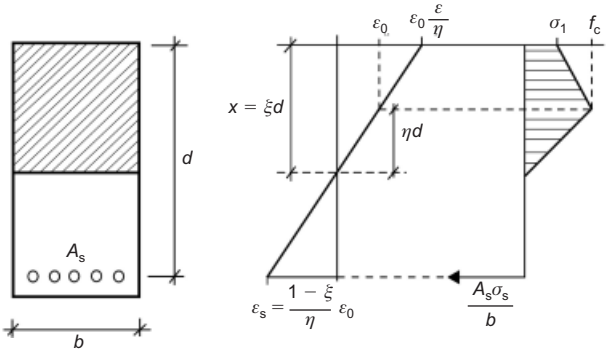

Figure 4. Diagrams of strains and stresses on a rectangular cross-section

$$\left(\varepsilon_0 \frac{\xi}{\eta} + \varepsilon_s\right) : d = \frac{\varepsilon_0\ \xi}{\eta} : \xi\ d \tag{3}$$

where η is a factor of proportionality which, multiplied by the effective depth d, provides the distance between the neutral axis and the point where $\sigma = f_c$, f_c being the concrete compressive strength. The deformation ε_s can therefore be expressed as a function of ε_0

$$\varepsilon_s = \frac{1 - \xi}{\eta}\ \varepsilon_0 \tag{4}$$

Moreover, σ_1/f_c is given by

$$\frac{\sigma_1}{f_c} = \frac{(\varepsilon_1/\xi) - \left[(\varepsilon_0\xi)/\eta\right]}{(\varepsilon_1/\xi) - \varepsilon_0} \tag{5}$$

The condition of force equilibrium in the longitudinal direction gives

$$F_c = F_s \tag{6}$$

where the resultant axial force of concrete in compression, F_c, is given by

$$F_c = \frac{1}{2} f_c \eta\ d\ b + \frac{1}{2}(\sigma_1 + f_c)\ (\xi\ d - \eta\ d)\ b \tag{7}$$

while the resultant of tensile steel, F_s, is given by

$$F_s = A_s \sigma_s \tag{8}$$

Equating Equations 7 and 8 and putting them in non-dimensional form by dividing them with respect to the product $b\ d\ f_c$, the following expression is finally obtained

$$\frac{A_s\ \sigma_s}{b\ d\ f_c} = \frac{1}{2}\ \left[\xi + \frac{\sigma_1}{f_c}(\xi - \eta)\right] \tag{9}$$

From rotational equilibrium about the reinforcement level, the bending moment M is obtained

$$M = \left(\frac{1}{2} f_c\ \eta\ d\ b\right)\left(d - \xi\ d + \frac{2}{3}\eta\ d\right) + \sigma_1(\xi\ d - \eta\ d)\ b \times \left[d - \frac{1}{2}(\xi\ d - \eta\ d)\right] + \frac{1}{2}(f_c - \sigma_1)\ (\xi\ d - \eta\ d) \times b\left[d - \frac{2}{3}(\xi\ d - \eta\ d)\right] \quad (10)$$

Then, in dimensionless form with respect to $b\ d^2 f_c$, it results in

$$\frac{6\ M}{b\ d^2 f_c} = \xi\ (3 - 2\ \xi + \eta) + \frac{\sigma_1}{f_c}(\xi - \eta)\ (3 - \xi + \eta) \quad (11)$$

The curvature $1/r$ is computed using the following expression

$$\frac{1}{r} = \frac{\varepsilon_0}{\eta\ d} \quad (12)$$

It is important to notice that the constitutive law proposed by Hillerborg for concrete in compression does not represent a material intrinsic property, but it depends on the depth of the compressive zone of concrete, $x = \xi\ d$, as can be seen from Figure 2. This dependence is found in the descending post-peak branch. Moreover, the considered softening branch results to be inversely proportional not only to x but also to the parameter β. While the influence of the compressive depth varies during the loading process, in Figure 5 it is possible to observe that, with the increase in the factor β, the last point of the softening branch moves towards left, that is $\varepsilon_1 = w_c/\beta\ d$ decreases.

As a consequence of this behaviour, the area under the post-peak branch decreases and the energy dissipated in the volume decreases. Therefore, the energy dissipated per unit volume predicted according to this model depends on the length of diffusion of crushing.

According to the overlapping crack model, for a brittle material with an elastic-softening behaviour, the energy is dissipated exclusively on the damaged surface and not in the volume of the undamaged material. Then, the energy which is globally spent to take the compressive specimen to failure, $\mathcal{G}_F A_0$, remains always constant, independently of the length of the specimen. Therefore, if in the stress–strain diagram the length of the base of measurement, ℓ_0, varies, as shown in Figure 6, there will be a single linear-elastic branch followed by a set of softening branches that tend to be close to the elastic branch when $\ell_0 \to \infty$. In fact, the area below such curves, being energy per unit volume, is inversely proportional to ℓ_0, because a constant amount of energy is dissipated in a larger and larger volume. Instead, when $\ell_0 \to 0$, the softening branch becomes horizontal.

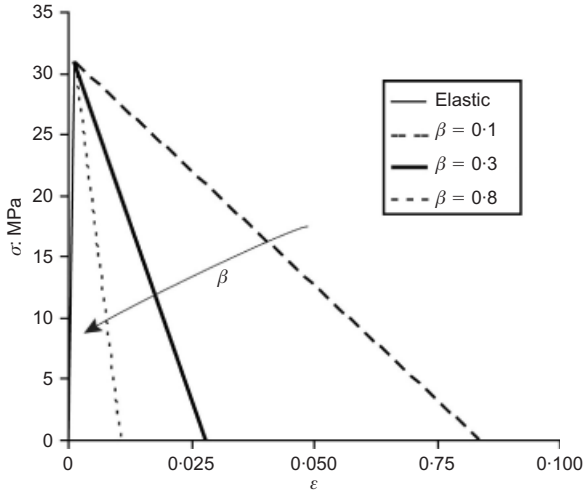

Figure 5. Influence of the parameter β on the constitutive law of concrete in compression, for h = 400 mm, $\rho = A_s'/b\ h = 1{\cdot}13\%$ and ξ = constant

Generalised analytical model

The analytical approach introduced by Hillerborg can be generalised by taking into account the additional contribution of the reinforcement in compression with area A_s' and positioned at a distance a from the beam extrados, as shown in Figure 7. According to Figure 7, the relationship of proportionality from similitude between triangles reads

$$\varepsilon_s' : (\xi\ d - a) = \frac{\varepsilon_0\ \xi}{\eta} : \xi\ d \quad (13)$$

Therefore, it can be written

$$\varepsilon_s' = \frac{\xi - (a/d)}{\eta}\ \varepsilon_0 \quad (14)$$

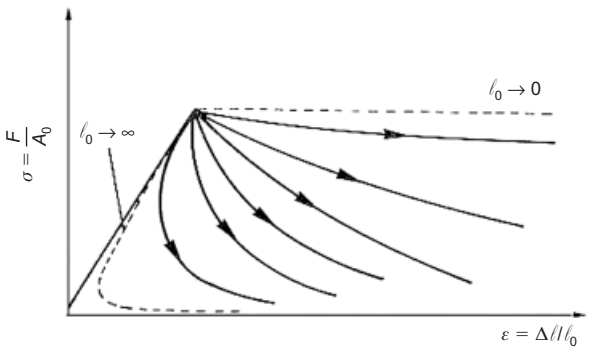

Figure 6. Stress–strain diagram varying the base of measurement ℓ_0 (area = $\mathcal{G}_F/\ell_0$)

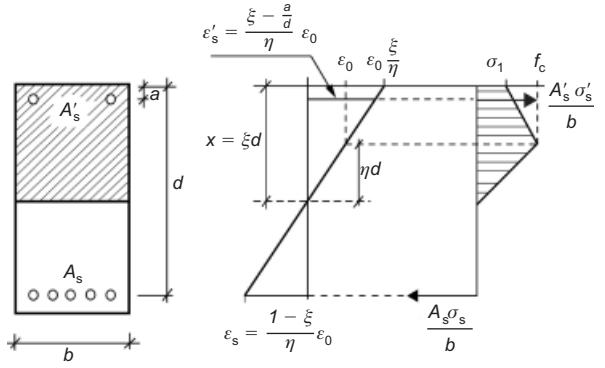

Figure 7. Strain and stress diagrams with compressive reinforcement

The force equilibrium in the longitudinal direction reads

$$F_c + F'_s = F_s \tag{15}$$

where the resultant of the concrete in compression, F_c, and that of the tensile steel, F_s, are given respectively by Equations 7 and 8, whereas the resultant of the compressive steel, F'_s, is obtained from the following relationship

$$F'_s = A'_s \sigma'_s \tag{16}$$

where σ'_s is the stress in the reinforcement at the extrados evaluated by considering its absolute value.

Substituting Equations 7, 8 and 16 into Equation 15 and turning Equation 15 into a non-dimensional form with respect to $b\ d\ f_c$, finally results in

$$\frac{A_s\ \sigma_s}{b\ d\ f_c} - \frac{A'_s\ \sigma'_s}{b\ d\ f_c} = \frac{1}{2}\left[\xi + \frac{\sigma_1}{f_c}\ (\xi - \eta)\right] \tag{17}$$

In addition, from rotational equilibrium with respect to the tensile reinforcement level, the bending moment M is obtained

$$\begin{aligned} M = {} & \left(\frac{1}{2} f_c\ \eta\ d\ b\right)\left(d - \xi\ d + \frac{2}{3}\eta\ d\right) \\ & + \sigma_1(\xi\ d - \eta\ d) \\ & \times b\left[d - \frac{1}{2}(\xi\ d - \eta\ d)\right] \\ & + \frac{1}{2}(f_c - \sigma_1)\ (\xi\ d - \eta\ d) \\ & \times b\left[d - \frac{2}{3}(\xi\ d - \eta\ d)\right] \\ & + \sigma'_s\ A'_s(d - a) \end{aligned} \tag{18}$$

Then, in dimensionless form with respect to $b\ d^2 f_c$, it can be written

$$\begin{aligned} \frac{6\ M}{b\ d^2 f_c} = {} & \xi\ (3 - 2\ \xi + \eta) \\ & + \frac{\sigma_1}{f_c}(\xi - \eta)\ (3 - \xi + \eta) \\ & + \sigma'_s\ A'_s\ (d - a)\frac{6}{b\ d^2 f_c} \end{aligned} \tag{19}$$

The procedure of solution is based on a series of steps which are summarised in the following list.

(*a*) *Step 1*. Definition of the geometrical characteristics of the cross-section, of the values of the mechanical properties (for example the concrete compression strength, f_c, the steel tensile strength, f_y, the concrete elastic modulus, E_c, and the steel elastic modulus, E_s), of the critical opening w_c and of the factor β.
(*b*) *Step 2*. Determination of x at the onset of crushing in the case of elastic behaviour of tensile and compressive steel according to Equation 15 with $F_c = (1/2) f_c x\ b$, then calculus of ξ as x/d, ε_s, ε'_s according to Equations 4 and 14, and ε_y as f_y/E_s.
(*c*) *Step 3*. If both reinforcements are in the elastic regime, η is set equal to ξ of step 2.
(*d*) *Step 4*. Reduce η as long as it is positive and, at each step, evaluate ε_s and ε'_s using Equations 4 and 14.
(*e*) *Step 5*. Check again the behaviour of both reinforcements, then compute the value of ξ using Equation 17.
(*f*) *Step 6*. If step 3 is not verified for one of the two reinforcements or for both, then x at the onset of crushing has to be evaluated consistently and then the first value of η. For the rest, steps 4, 5 and 6 follow.
(*g*) *Step 7*. Find the real value of ξ from the third-order polynomial Equation 17.
(*h*) *Step 8*. Check of the ultimate limit of strain for the tensile and compressive steel.
(*i*) *Step 9*. Computation of the bending moment, M, by means of Equation 19, the curvature using Equation 12, and the rotation as h/r.
(*j*) *Step 10*. Plot the bending moment–rotation diagram.

Figure 8 shows the variation of ξ, related to the depth of the compressive zone of concrete, $x = \xi\ d$, of the strain of the reinforcement at the lower tensile edge, ε_s, and of the strain of the reinforcement at the upper compressive edge, ε'_s, as functions of η in the case of low percentage of reinforcement ($\rho = 0{\cdot}28\%$). The loading process is controlled by means of the coefficient η, which, multiplied by the effective depth d, provides the distance between the position of the neutral axis and the point of the compressive zone of concrete where $\sigma = f_c$. Since this parameter is progressively reduced in the simulation, it starts from $\eta = \xi_0$, where ξ_0 corresponds to ξ at the onset of

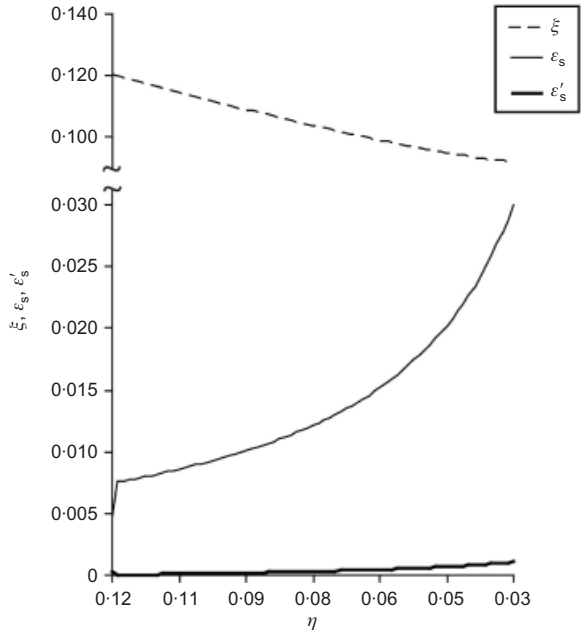

Figure 8. Trends of ξ, ε_s and ε'_s for a low reinforcement percentage ($\rho = 0{\cdot}28\%$) and $h = 400$ mm

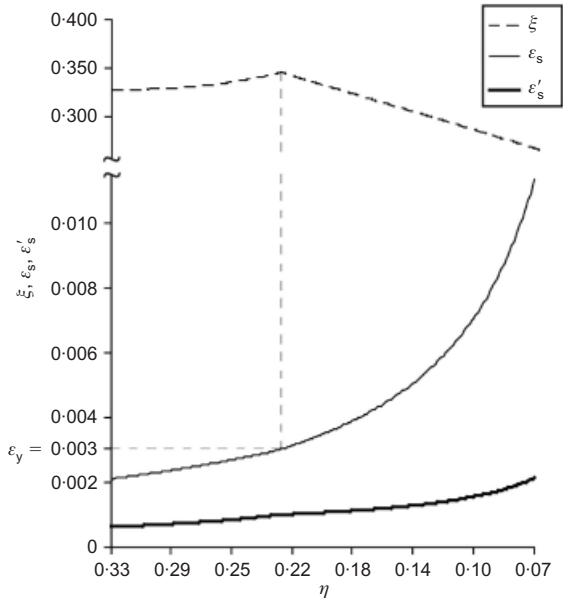

Figure 9. Trends of ξ, ε_s and ε'_s for a high reinforcement percentage ($\rho = 1{\cdot}13\%$) and $h = 400$ mm

crushing, and then progressively diminishes until $\xi - (\xi_0 - \eta) > 0$, that is until the value of η is not larger than ξ. In the case of a low reinforcement percentage, as shown in Figure 8, the non-dimensional depth of compressive concrete, ξ, is an increasing function of η, whereas an opposite trend is observed for ε_s and ε'_s. The reinforcement at the tensile side yields when the strain of yielding is reached, $\varepsilon_y = 3‰$, then it provides a constant tensile resultant F_s. On the other hand, at the extrados, the compressive resultant of the reinforcement is not limited. This is consistent with the experimental observation in low-reinforced beams.

In the case of high reinforcement percentage ($\rho = 1{\cdot}13\%$), Figure 9, while ε_s and ε'_s are still increasing during the simulation controlled by the reduction of η, ξ increases for $\varepsilon_s < \varepsilon_y$ and then decreases for $\varepsilon_s > \varepsilon_y$. For $\varepsilon_s < \varepsilon_y$, the depth of the compressive concrete zone increases since at the same time the tensile resultant of tensile reinforcement increases, having to satisfy the force equilibrium in the longitudinal direction expressed by Equation 15. When the tensile steel yielding is reached, this resultant becomes constant while ξ decreases consistently with the moment reduction. The reinforcement at the compressive edge presents a strain level higher than that for the low-reinforcement case (see Figure 8). Here, the strain level tends to the yield point.

Numerical examples and comparison with experimental results

The numerical predictions obtained using the generalised Hillerborg's model are herein compared with the experimental results by Bosco and Debernardi (1992). Two loading schemes were considered: one concentrated force in the middle-span position, or three concentrated forces applied on a central element in the middle of the beam. In this section, the data related to the former test condition are consisdered. The properties of the high-ductility steel are: $f_y = 600$ MPa, $E_s = 200$ GPa and $\upsilon = 0{\cdot}3$. The concrete compressive strength, f_c, is equal to 30·9 MPa. In spite of the presence of stirrups in the tested beams, they are not modelled in the present study, although they exert a confinement to concrete in the compressed zone.

The scheme of the considered cross-sections with total depth H equal to 200, 400 and 600 mm is shown in Figure 10. The percentage of tensile reinforcement $\rho = A_s/(b\ H)$ is varied from 0·13% to 1·70%. The slenderness is taken as constant and equal to $L/H = 10$, where L is the span of the beam. In the beams there is also reinforcement in compression (see Table 1).

The moment–rotation diagram of an RC beam with a depth of 400 mm and a percentage ρ of tensile reinforcement equal to 0·28% is shown in Figure 11. In this

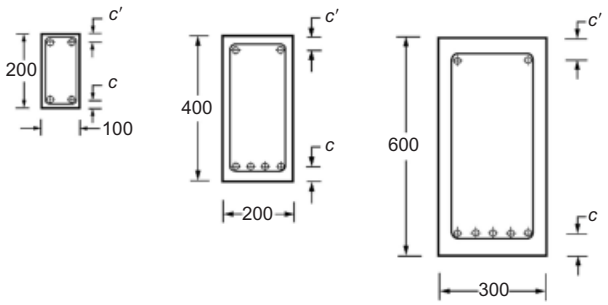

Figure 10. Geometry of the cross-sections (dimensions in mm)

Table 1. Geometrical characteristics of the specimens

Beam type	h: mm	ℓ: mm	b: mm	Tensile reinforcement	ρ: %	c: mm	Compressive reinforcement	ρ_c: %	c': mm
T1A1	200	2000	100	1 Φ 12	0·57	24	1 Φ 8	0·25	22
T2A1	200	2000	100	2 Φ 12	1·13	24	2 Φ 8	0·50	22
T3A1	200	2000	100	3 Φ 12	1·70	24	2 Φ 8	0·50	22
T4A1	400	4000	200	2 Φ 12	0·28	35	2 Φ 10	0·20	45
T5A1	400	4000	200	4 Φ 12	0·57	35	2 Φ 10	0·20	45
T6A1	400	4000	200	8 Φ 12	1·13	40	2 Φ 10	0·20	45
T7A1	400	4000	200	12 Φ 12	1·70	50	2 Φ 12	0·28	45
T8A1	600	6000	300	2 Φ 12	0·13	35	2 Φ 12	0·13	70
T9A1	600	6000	300	4 Φ 12	0·25	35	2 Φ 12	0·13	70
T10A1	600	6000	300	9 Φ 12	0·57	35	2 Φ 12	0·13	70
T11A1	600	6000	300	18 Φ 12	1·13	50	2 Φ 12	0·13	70

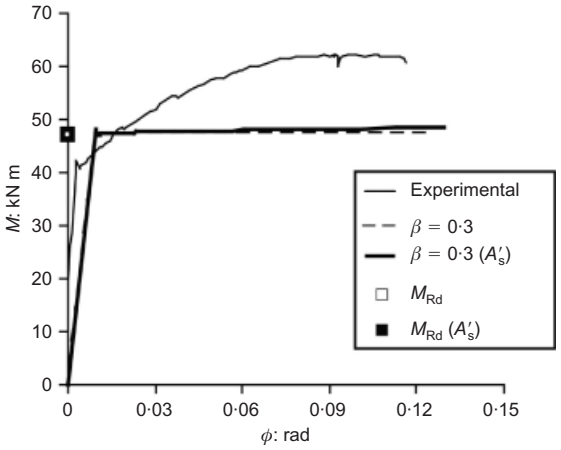

Figure 11. Effect of reinforcement in compression for $h = 400$ mm and $\rho = 0{\cdot}28\%$ (experimental data taken from Bosco and Debernardi (1992))

diagram, the experimental curve (solid line), the analytical prediction corresponding to $\beta = 0{\cdot}3$ without reinforcement in compression (dashed line) and the analytical prediction with $\beta = 0{\cdot}3$ with reinforcement in compression (thicker solid line) are compared. Moreover, the values of the resistant moment at the ultimate limit state are reported according to Eurocode 2 (CEN, 2004). The value of M_{Rd} evaluated in the absence of reinforcement in the compressive zone is reported with a white square dot, while in presence of A'_s, M_{Rd} is reported with a black square dot. In this case the parameter β does not influence the loading capacity of the beam and, for low reinforcement percentages, it affects in a negligible manner the plastic rotation capacity. The reason is that, in the case of low reinforcement percentages, the influence of cracking in tension prevails on the crushing phenomenon in compression. In addition, it can be observed that, in the case of low-reinforced beams, there is no particular difference between the presence or the absence of steel in the compressive zone as regards the ultimate moment and the extension of the plastic plateau. The values of the resistant moment at the ultimate limit state are well approximated by the respective values of the moment of the plastic plateau, estimated according to the original and the generalised Hillerborg's model. On the other hand, the experimental curve in the solid line shows a hardening behaviour very likely due to the non-linear response of steel in tension.

The moment–rotation diagram for an RC beam with a depth of 400 mm and a percentage of reinforcement ρ equal to 1·13% is shown in Figure 12. In this diagram, the experimental curve (dotted line) is compared with the analytical prediction corresponding to $\beta = 0{\cdot}3$ without reinforcement in compression (solid line), the analytical prediction with $\beta = 0{\cdot}3$ and with reinforcement in compression (dashed line); also the analytical prediction with $\beta = 0{\cdot}55$ and with reinforcement in compression (thicker solid line). The values of the resistant moment at the ultimate limit state are also shown. The value of M_{Rd} evaluated in the absence of reinforcement in the compressive zone is reported with a white square symbol, while in the presence of A'_s, M_{Rd} is reported with a black square symbol. Also in

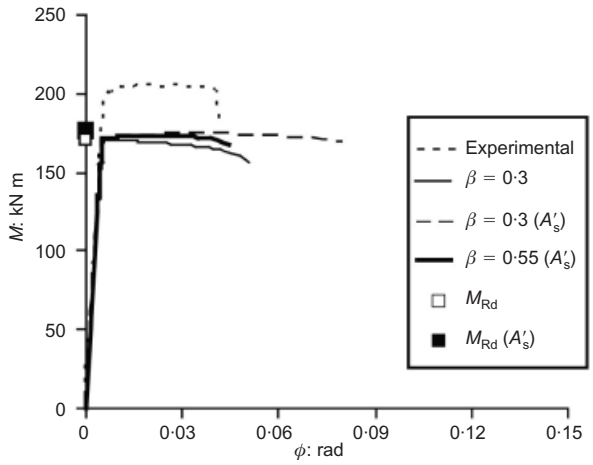

Figure 12. Effect of reinforcement in compression for $h = 400$ mm and $\rho = 1{\cdot}13\%$ (experimental data taken from Bosco and Debernardi (1992))

this case, and regardless of the amount of reinforcement, the parameter β does not influence the bearing capacity of the beam, since the resistant moment does not change by varying β from 0·3 to 0·55. Moreover, it is possible to observe that, in the case of a high percentage of reinforcement, the generalised Hillerborg's model with $\beta = 0{\cdot}55$ and with reinforcement in compression provides a better approximation to the experimental results. The moment plotted against rotation theoretical curve without A'_s interprets the experimental response well if factor β is taken as equal to 0·3. If some reinforcement in compression is added with $\beta = 0{\cdot}3$, a longer plastic plateau and an unchanged value of the resistant moment are found. Hence, the addition of A'_s determines an increase in ductility, that is a greater value of plastic rotation. It is necessary to use a higher value of β in order to match the experimental plastic rotation. It can be seen that the presence of the reinforcement in compression does not influence the value of the moment at the elastic limit. On the other hand, accounting for this contribution can determine an increase in the extent of the plastic branch, developing a greater plastic rotation and, consequently, a higher structural ductility. In any case, no size-scale effect is revealed in the analysis of the parameter β.

The plastic rotation, ϕ_p, computed as the difference between the final rotation and the rotation at the elastic limit, is plotted as a function of β for different beam depths, h, and for three reinforcement percentages, $\rho = 0{\cdot}5\%$, 1% and 2% in Figures 13–15. In each of the three figures, case (a) refers to the presence of reinforcement in tension only, while case (b) also considers reinforcement in compression. The values of ρ_c have been chosen in order to match the experimental data in Table 1. Generally, it is possible to observe that, as β increases, the values of plastic rotations decrease – that is, the plastic branches shorten. This trend is even more evident in the case of $\rho = 1\%$ and $\rho = 2\%$ – that is, for high reinforcement percentages. On the other hand, it is possible to observe that, as a limit case, for $\rho = 0{\cdot}5\%$ and $h = 200$ mm, the curve presents a slope equal to zero, since the model is not so effective in the case of low reinforcement ratios. Moreover, by increasing the depth of the beam, the plastic rotation decreases. This means that an increase of the size-scale determines a more brittle behaviour resulting in shorter and shorter plastic branches. This trend shows clearly a strong effect of the size-scale on the rotational capacity of RC beams in bending, as was also found experimentally by Bosco and Debernardi (1992). Actually, brittleness also depends significantly on the reinforcement percentage and can be a symptom of a deficit of ρ, and so of a problem of minimum reinforcement; on the other hand, it can indicate an excessive value of ρ and so a case of over-reinforcement. As a general comment, the plastic branches in the presence of reinforcement in compression are longer than those observed when $A'_s = 0$.

The moment–rotation diagrams for a constant percentage of reinforcement $\rho = 1{\cdot}13\%$ and varying the height of the section $h = 200$, 400 and 600 mm is shown in Figure 16. These diagrams show the theoretical versus experimental results comparison between the results obtained by Bosco and Debernardi (1992) and the analytical responses obtained using the Hillerborg's generalised model with $\beta = 0{\cdot}55$. It can be seen that, with increasing the beam depth, a gradual brittleness of the structural behaviour appears, characterised by higher values of plastic moment and shorter plastic branches.

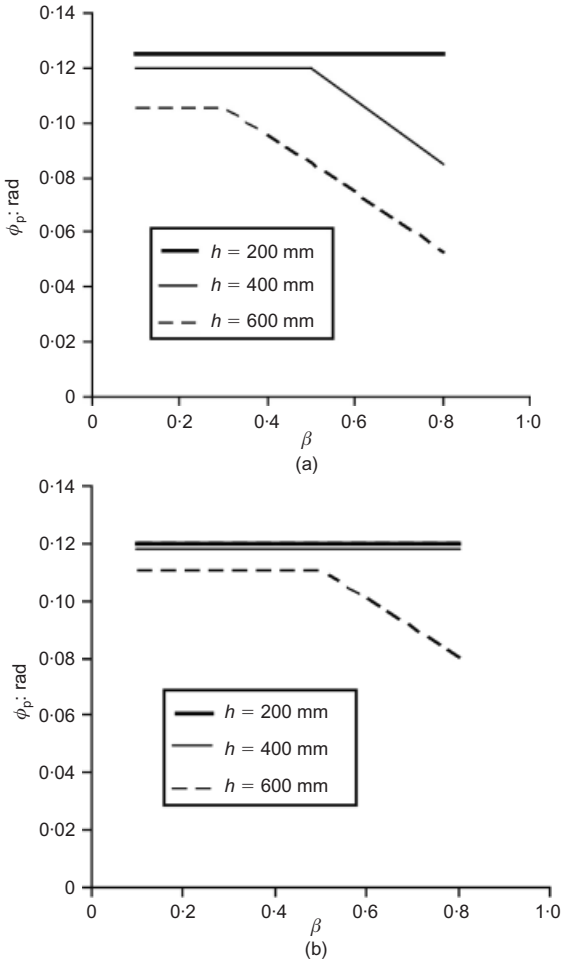

Figure 13. Influence of β on the structural response for $\rho = 0{\cdot}5\%$; (a) $\rho_c = 0\%$ and (b) $\rho_c = 0{\cdot}5\%$ ($h = 200$ mm), 0·2% ($h = 400$ mm) and 0·13% ($h = 600$ mm)

The moment–rotation diagrams for a constant beam depth, $h = 200$ and 400 mm, and varying the reinforcement percentage ρ, are shown in Figures 17 and 18. In these diagrams, the theoretical against experimental results comparison is shown between the results by Bosco and Debernardi (1992) and the analytical responses of the generalised Hillerborg's model obtained with $\beta = 0{\cdot}55$. A progressive embrittlement of the structural response by increasing the percentage of tensile reinforcement can be seen, with the appearance of higher values of moments at the plastic plateau and shorter plastic branches.

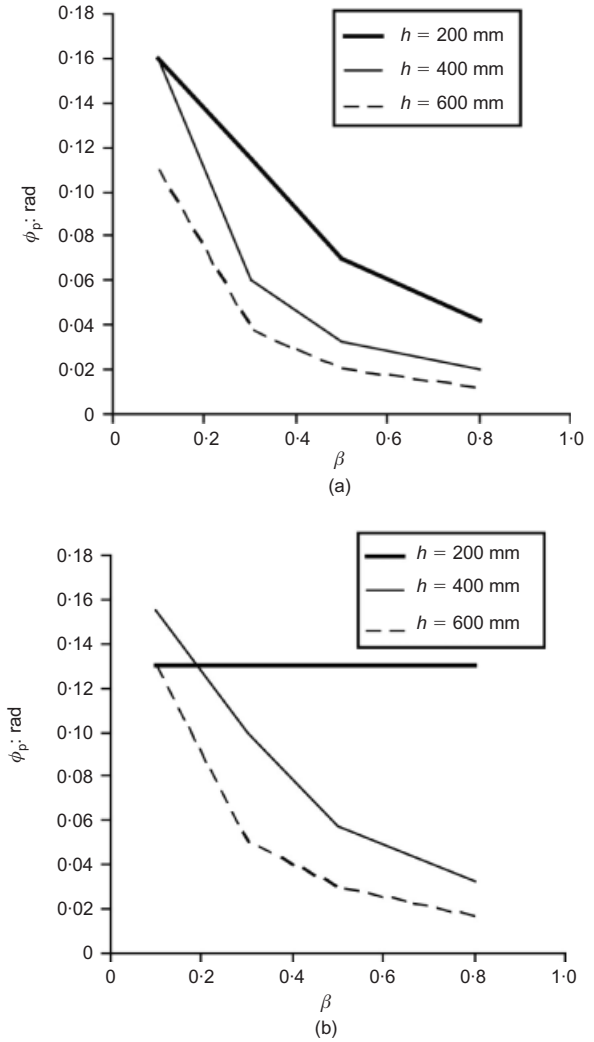

Figure 14. Influence of β on the structural response for ρ = 1%; (a) $\rho_c = 0\%$ and (b) $\rho_c = 0{\cdot}5\%$ (h = 200 mm), 0·2% (h = 400 mm) and 0·13% (h = 600 mm)

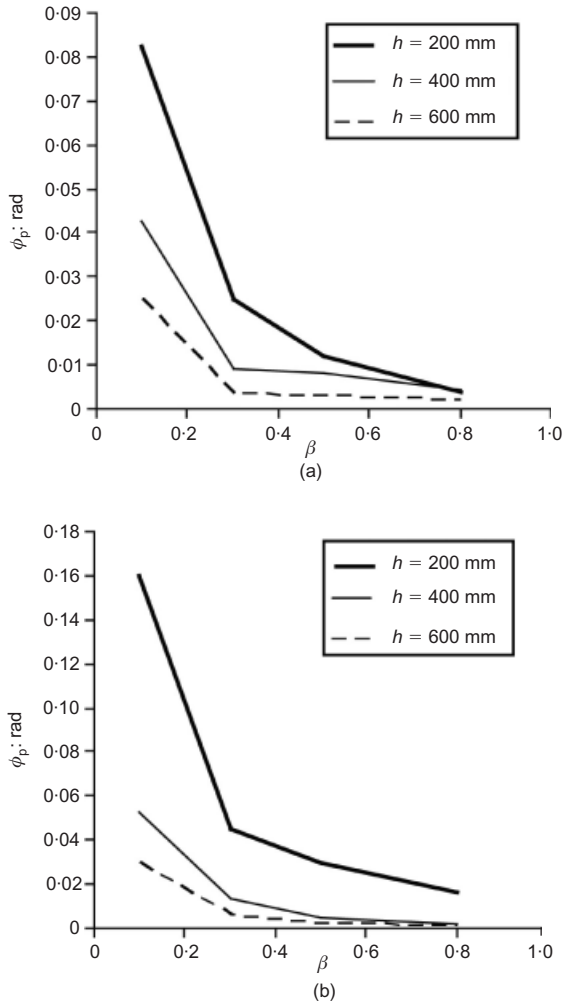

Figure 15. Influence of β on the structural response for ρ = 2%; (a) $\rho_c = 0\%$ and (b) $\rho_c = 0{\cdot}5\%$ (h = 200 mm), 0·2% (h = 400 mm) and 0·13% (h = 600 mm)

Discussion and conclusions

In the present work, the Hillerborg's model has been generalised considering also reinforcement in compression and this has permitted an effective experimental comparison in order to set the input parameters used in the model.

In the original Hillerborg's model (Hillerborg, 1990), the length of the localisation zone was assumed to be proportional to the compression depth. However, although Hillerborg suggested $\beta = 0{\cdot}8$, this choice did not receive an experimental confirmation. In the present paper, this parameter was set on an experimental basis and it was found necessary to use a lower value of β to achieve a good agreement with experiments. In the more general case of presence of steel also in compression, β has to be set approximately equal to 0·55.

This reduction of β is also in agreement with the overlapping crack model recently proposed by Carpinteri *et al.* (2007), which assumes the development of strain localisation in compression as a material

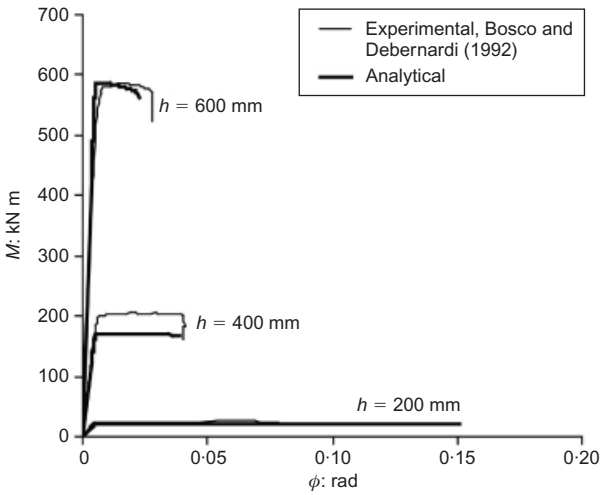

Figure 16. Structural response varying the height of the section for ρ = 1·13% and β = 0·55

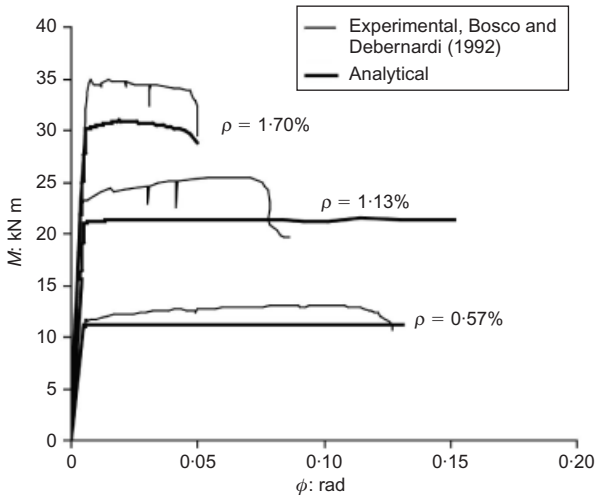

Figure 17. Structural response by varying the reinforcement percentage, for $h = 400$ mm, $\beta = 0{\cdot}55$ and $\rho_c = 0{\cdot}2\%$

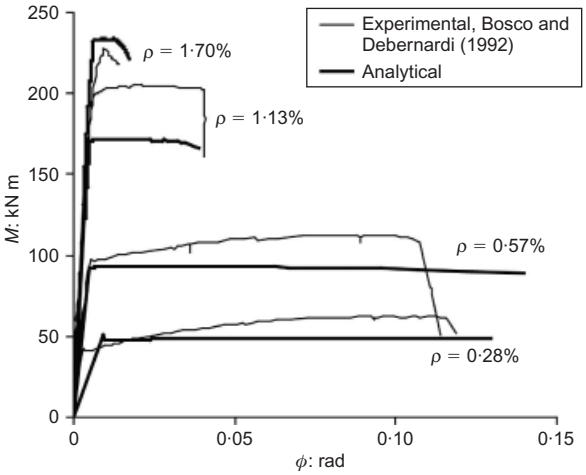

Figure 18. Structural response by varying the tensile reinforcement percentage, for $h = 200$ mm, $\beta = 0{\cdot}55$ and $\rho_c = 0{\cdot}5\%$

interpenetration. This limit situation would in fact correspond to $\beta \to 0$. Hence, this confirms the local nature of the physical phenomenon of concrete crushing in compression.

The values of plastic rotation, ϕ_p, are shown in Figure 19 by varying the beam depth, h, and the reinforcement percentage, ρ. This figure shows the theoretical against experimental results comparison between the results by Bosco and Debernardi (1992) and the analytical predictions obtained by applying the generalised Hillerborg's model with $\beta = 0{\cdot}55$. It can be observed that, by increasing the beam depth and/or the reinforcement percentage, the plastic rotation decreases, with the appearance of brittleness in the structural response. No size-scale effect is revealed in the analysis of the parameter β. Moreover, it can be observed that the analytical Hillerborg's model gives a very good approximation to the experimental results for high values of the reinforcement percentage, while the

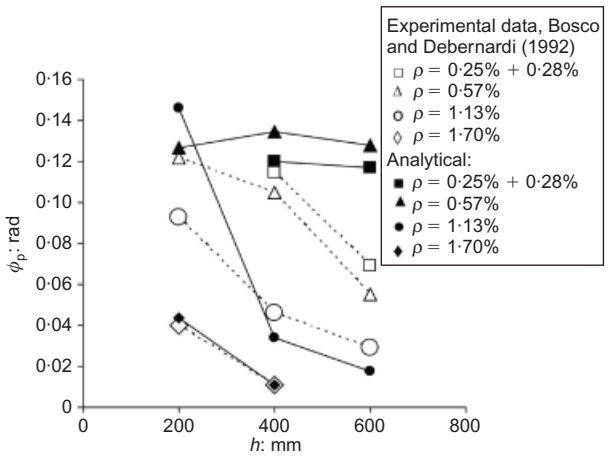

Figure 19. Theoretical against experimental comparison in terms of plastic rotations

model is not fully adequate when addressing cases with low reinforcement percentages. This is because the model does not take into account the cohesive behaviour of concrete in tension, whose contribution is relevant for low-reinforcement RC beams.

These results imply that the proposed generalised Hillerborg model can be suitably applied in the case of over-reinforced beams, where concrete crushing is the prevailing non-linearity. The proposed model is therefore able to capture the phenomenon of size-scale ductile-to-brittle transition.

The theoretical against experimental results comparisons have highlighted the innovative aspects of the proposed theoretical approach, which has the great advantage of providing closed-form solutions that are of practical interest for design codes. On the other hand, more sophisticated numerical models, such as the overlapping crack model (Carpinteri *et al.*, 2007), must be involved when the full range of mechanical responses has to be predicted.

Acknowledgements

The financial support of the European Union to the Leonardo da Vinci Project I/06/B/F/PP-154069 'Innovative learning and training on fracture (ILTOF)' is gratefully acknowledged.

References

Bosco C and Debernardi PG (1992) *Experimental Investigation on the Ultimate Rotational Capacity of RC Beams*. Atti Dipartimento di Ingegneria Strutturale, Politecnico di Torino, Report No. 36.

Carpinteri A (1984) Stability of fracturing process in RC beams. *Journal of Structural Engineering, ASCE* **110(3)**: 544–554.

Carpinteri A (1989) Cusp catastrophe interpretation of fracture instability. *Journal of the Mechanics and Physics of Solids* **37(5)**: 567–582.

Carpinteri A, Corrado M, Paggi M and Mancini G (2007) Cohesive versus overlapping crack model for a size effect analysis of RC

elements in bending. *Proceedings of the 6th International Conference on Fracture Mechanics of Concrete and Concrete Structures (FraMCoS-6), Catania, Italy*: *Design, Assessment and Retrofitting of RC Structures* **6(2)**: 655–663. Taylor & Francis.

CEN (European Committee for Standardization) (2004) Eurocode 2: Design of concrete structures. Part 1-1: General rules and rules for buildings. European Committee for Standardization, Brussels, ENV 1992-1-1.

Hillerborg A (1990) Fracture mechanics concepts applied to moment capacity and rotational capacity of reinforced concrete beams. *Engineering Fracture Mechanics* **35(11)**: 233–240.

van Mier JGM (1984) *Strain-softening of Concrete under Multiaxial Loading Conditions*. PhD thesis, Eindhoven University of Technology, the Netherlands.

Discussion contributions on this paper should reach the editor by 1 February 2011